ECONSTOR
Make Your Publications Visible.

A Service of

ZBW Leibniz-Informationszentrum Wirtschaft
Leibniz Information Centre for Economics

Zhang, Yachao et al.

Article

Interval optimization based coordination scheduling of gas-electricity coupled system considering wind power uncertainty, dynamic process of natural gas flow and demand response management

Energy Reports

Provided in Cooperation with:
Elsevier

Suggested Citation: Zhang, Yachao et al. (2020) : Interval optimization based coordination scheduling of gas-electricity coupled system considering wind power uncertainty, dynamic process of natural gas flow and demand response management, Energy Reports, ISSN 2352-4847, Elsevier, Amsterdam, Vol. 6, pp. 216-227, https://doi.org/10.1016/j.egyr.2019.12.013

This Version is available at:
https://hdl.handle.net/10419/244025

Standard-Nutzungsbedingungen:

Die Dokumente auf EconStor dürfen zu eigenen wissenschaftlichen Zwecken und zum Privatgebrauch gespeichert und kopiert werden.

Sie dürfen die Dokumente nicht für öffentliche oder kommerzielle Zwecke vervielfältigen, öffentlich ausstellen, öffentlich zugänglich machen, vertreiben oder anderweitig nutzen.

Sofern die Verfasser die Dokumente unter Open-Content-Lizenzen (insbesondere CC-Lizenzen) zur Verfügung gestellt haben sollten, gelten abweichend von diesen Nutzungsbedingungen die in der dort genannten Lizenz gewährten Nutzungsrechte.

Terms of use:

Documents in EconStor may be saved and copied for your personal and scholarly purposes.

You are not to copy documents for public or commercial purposes, to exhibit the documents publicly, to make them publicly available on the internet, or to distribute or otherwise use the documents in public.

If the documents have been made available under an Open Content Licence (especially Creative Commons Licences), you may exercise further usage rights as specified in the indicated licence.


https://creativecommons.org/licenses/by-nc-nd/4.0/

WWW.ECONSTOR.EU

Mitglied der Leibniz-Gemeinschaft

Energy Reports 6 (2020) 216–227

Contents lists available at ScienceDirect

Energy Reports

journal homepage: www.elsevier.com/locate/egyr

Research paper

Interval optimization based coordination scheduling of gas–electricity coupled system considering wind power uncertainty, dynamic process of natural gas flow and demand response management

Yachao Zhang [a], Zhanghao Huang [a], Feng Zheng [a,*], Rongyu Zhou [b], Xueli An [b], Yinghai Li [c]

[a] Fujian Smart Electrical Engineering Technology Research Center, School of Electrical Engineering and Automation, Fuzhou University, Fuzhou 350108, China
[b] China Institute of Water Resources and Hydropower Research, Beijing 100038, China
[c] College of hydraulic and environmental engineering, China Three Gorges University, Yichang 443002, China

ARTICLE INFO

Article history:
Received 20 October 2019
Received in revised form 2 December 2019
Accepted 13 December 2019
Available online xxxx

Keywords:
Gas–electricity coupled system
Coordination scheduling
Interval optimization
Demand response management
Wind power uncertainty

ABSTRACT

With the remarkable growth of natural gas consumption and the development of renewable energy worldwide in recent years, the penetration capacity of gas-fired generators and uncertain renewable energy has significantly become larger, which poses a great challenge to the reliable and economic operation of the gas–electricity interconnected system. This paper proposes an interval optimization based coordination scheduling model for the gas–electricity coupled system considering the dynamic characteristics of natural gas flow, wind power integration and demand response management. By introducing the arithmetic and order relation of interval numbers, the objective function and corresponding constraints for the interval-based dispatch model can be converted into the deterministic expressions with degrees of pessimism, then the proposed model can be solved in the master-subproblem framework. On this basis, two case studies are implemented on the 6-bus power system integrated with 6-node natural gas system and the modified IEEE 118-bus system with 10-node natural gas system to investigate the impact of gas flow dynamic process, demand response management, wind power uncertainty on the scheduling solution of the coupled systems. Moreover, the scenario-based stochastic optimization and robust optimization methods are carried out for comparison. Simulation results demonstrate the effectiveness of the proposed interval optimization method.

© 2020 The Authors. Published by Elsevier Ltd. This is an open access article under the CC BY-NC-ND license (http://creativecommons.org/licenses/by-nc-nd/4.0/).

1. Introduction

With the remarkable increase of natural gas consumption in the last decade, the integrated energy system (IES) coupling natural gas system with power system has gained growing attention (Chaudry et al., 2008). As the critical linkage component between power network and natural gas network, the gas-fired unit is preferred due to the quick response ability and lower pollution emissions compared with the thermal unit (Liu et al., 2009a). However, it poses a serious challenge to the reliable and economic operation of the IES when the penetration capacity of gas-fired unit becomes larger (Liu et al., 2010). As a result, the interdependence between natural gas system and electricity system should be considered for the coordination scheduling of the IES (Liu et al., 2009b; Zhang et al., 2015).

On the other hand, the integration of renewable energy will have a direct influence on the safe and stable operation of power system due to its uncertainty (Nasrolahpour and Ghasemi, 2015; Xiao et al., 2015). On this account, the coordinated optimal scheduling of gas–electricity integrated system is facing greater challenges with consideration of renewable energy uncertainty (Qin et al., 2015; He and Li, 2018). The short-term scheduling of the IES considering wind power has been studied by many researchers. A bi-level economic dispatch model for gas–electricity coupled system with wind power is proposed, yet wind power uncertainty is not taken into account (Li et al., 2017). The scenario-based stochastic programming is employed to deal with wind power uncertainty for the IES (Qadrdan et al., 2013; Alabdulwahab et al., 2015; Li et al., 2018), in which the accurate probability distribution of wind power forecast error is difficult to acquire. The scenario adjustable scheduling model with robust constraints is established (Liu and Gao, 2017). A robust optimization methodology is proposed for the wind-thermal system considering natural gas availability constraints (Liu et al., 2014). Two-stage robust optimization is utilized in power system with wind power (Jiang et al., 2012; Dehghan et al., 2014), and a robust stochastic optimization model is proposed to overcome

* Corresponding author.
E-mail address: zf@fzu.edu.cn (F. Zheng).

https://doi.org/10.1016/j.egyr.2019.12.013
2352-4847/© 2020 The Authors. Published by Elsevier Ltd. This is an open access article under the CC BY-NC-ND license (http://creativecommons.org/licenses/by-nc-nd/4.0/).

wind power uncertainty (Tan et al., 2015). Robust optimization can provide a robust solution in the worse-case scenario, but the scheduling decision may be so conservative that the operation economy is sacrificed. Besides, the generation scheduling problem with large scale wind farms is solved by a fuzzy optimization-based method (Siahkali and Vakilian, 2010).

As an effective alternative to deal with uncertain variables, interval analysis is proposed by Moore (Moore, 1979). With no need of the probability distribution information for uncertainties, the interval-based optimization method only needs the lower and upper bound for the uncertain variables. Interval optimization is adopted to handle wind power uncertainty for the electricity–gas coupled system in (Bai et al., 2016; Qiao et al., 2017). However, the dynamic process in natural gas transmission network is not considered in the above interval-based optimization models.

The transient-state model of natural gas system is built as a group of partial differential equations and algebraic equations (Liu et al., 2011). And the steady-state and transient-state operation scenes of the gas–electricity integrated system are simulated (Correa-Posada and Sánchez-Martín, 2015). It indicates that the dynamic process of gas flow has a prominent influence on the available gas quantity by gas-fired units.

In addition, the literatures above implement different approaches to obtain the dispatch solutions for the coordination scheduling of the IES, which is a nonlinear and non-convex optimization problem. Compared with MINLP, MILP shows fast and robust performance in solving and has the potential of finding the global optimal solution (Geißler et al., 2012; Correaposada and Sánchez-Martín, 2014).

In the above reported literatures, some studies concern the impact of natural gas system on power system economic dispatch, some researches concentrate on dealing with wind power uncertainty, and others focus on the transient-state modeling of natural gas system. However, there is no study to model the gas–electricity integrated system considering the dynamic process of gas network, dealing with wind power uncertainty with demand response management as well as adopting synergetic strategies to improve operation reliability and economy for the IES.

As a result, the purpose of this study is to formulate a coordination scheduling model for the gas–electricity coupled system considering wind power uncertainty. Due to the transient characteristics of gas flow, the dynamic process of gas flow is taken into account when modeling natural gas system. Moreover, an interval optimization (IO) method is proposed to handle wind power uncertainty. By introducing the arithmetic and order relation of interval numbers, the objective of interval optimization is to achieve the optimal mid-point and width simultaneously. The constraints containing interval variables can be transformed into deterministic constraints reflecting the degree of pessimism. In addition, the demand side management for residential gas load and electric load can be integrated into the coordination scheduling model to improve the reliability and economy of the IES.

The main contributions of this paper can be summarized as follows:

(1) the deterministic dispatch model for gas–electricity coupled system is established in the light of different application cases to investigate the impact of gas dynamic process and demand response on the scheduling solution of the IES;

(2) the interval optimization method based on interval order relation is proposed to model the IES for the first time, which provides a practical and effective way to handle wind power uncertainty;

(3) performance of the proposed interval optimization method, the scenario-based stochastic optimization method and the robust optimization method is compared for two test systems with different scales. Simulation results demonstrate the superiority of proposed method for handling the optimization problem with uncertainties.

The rest of this paper is organized as follows. Section 2 introduces the basic arithmetic and order relation of interval numbers. Section 3 describes the models of the gas–electricity integrated system and the demand response strategies for different loads in details. Section 4 presents the deterministic optimization model and interval optimization model for the coordination scheduling of the IES. Section 5 presents the case studies in two different gas–electricity interconnected test systems. Finally, the conclusions are drawn in Section 6.

2. Arithmetic and order relation of interval numbers

2.1. The basic arithmetic of interval numbers

An interval number represents the set of all possible values that a random variable may take by means of the left and right limits. The interval mathematics defines two important representations of interval numbers as follows:

$$\boldsymbol{A} = \left[a^{\mathrm{L}},\ a^{\mathrm{R}}\right] = \left\{a \,|a^{\mathrm{L}} \le a \le a^{\mathrm{R}}\right\} \tag{1}$$

where a^{L} is the left limit of interval number $\boldsymbol{A}$ and a^{R} is the right limit of $\boldsymbol{A}$. If $a^{\mathrm{L}} = a^{\mathrm{R}} = a$, the interval number $\boldsymbol{A}$ will degenerate into a real number a. Consequently, interval numbers can be regarded as the extension of real numbers.

Alternatively, $\boldsymbol{A}$ can be defined as:

$$\boldsymbol{A} = \langle m(\boldsymbol{A}),\ w(\boldsymbol{A})\rangle = \{a \,|m(\boldsymbol{A}) - w(\boldsymbol{A}) \le a \le m(\boldsymbol{A}) + w(\boldsymbol{A})\} \tag{2}$$

where $m(\boldsymbol{A})$ and $w(\boldsymbol{A})$ denote the midpoint and width of interval number $\boldsymbol{A}$, respectively. $m(\boldsymbol{A})$ represents the most reasonable value while $w(\boldsymbol{A})$ reflects the uncertainty level.

Combined Eqs. (1) and (2), $m(\boldsymbol{A})$ and $w(\boldsymbol{A})$ can be expressed by:

$$\begin{aligned} m(\boldsymbol{A}) &= (a^{\mathrm{R}} + a^{\mathrm{L}})/2 \\ w(\boldsymbol{A}) &= (a^{\mathrm{R}} - a^{\mathrm{L}})/2 \end{aligned} \tag{3}$$

In addition, the uncertainty of interval number $\boldsymbol{A}$ can be defined as:

$$\gamma(\boldsymbol{A}) = \frac{w(\boldsymbol{A})}{|m(\boldsymbol{A})|},\ m(\boldsymbol{A}) \ne 0 \tag{4}$$

Assuming that λ is a constant and $\boldsymbol{B} = [b^{\mathrm{L}},\ b^{\mathrm{R}}]$, the scalar multiplication, the extended addition and subtraction for interval numbers can be defined as follows (Liu et al., 2017):

$$\lambda \cdot \boldsymbol{A} = \begin{cases} [\lambda a^{\mathrm{L}}, \lambda a^{\mathrm{R}}] \text{ if } \lambda \ge 0 \\ [\lambda a^{\mathrm{R}}, \lambda a^{\mathrm{L}}] \text{ if } \lambda < 0 \end{cases} \tag{5}$$

$$\lambda + \boldsymbol{A} = [\lambda + a^{\mathrm{L}},\ \lambda + a^{\mathrm{R}}] \tag{6}$$

$$\boldsymbol{A} + \boldsymbol{B} = [a^{\mathrm{L}} + b^{\mathrm{L}},\ a^{\mathrm{R}} + b^{\mathrm{R}}] \tag{7}$$

$$\boldsymbol{A} - \boldsymbol{B} = [a^{\mathrm{L}} - b^{\mathrm{R}},\ a^{\mathrm{R}} - b^{\mathrm{L}}] \tag{8}$$

$$m(\boldsymbol{A} + \boldsymbol{B}) = m(\boldsymbol{A}) + m(\boldsymbol{B}) \tag{9}$$

$$m(\boldsymbol{A} - \boldsymbol{B}) = m(\boldsymbol{A}) - m(\boldsymbol{B}) \tag{10}$$

$$w(\boldsymbol{A} + \boldsymbol{B}) = w(\boldsymbol{A} - \boldsymbol{B}) = w(\boldsymbol{A}) + w(\boldsymbol{B}) \tag{11}$$

2.2. The order relation of interval numbers

The order relation of interval numbers is introduced to compare the different interval numbers. Assume that $\boldsymbol{A}$ and $\boldsymbol{B}$ are two interval objective values for the minimization problem and the midpoint of $\boldsymbol{A}$ is not larger than that of $\boldsymbol{B}$ as shown in Eq. (12),

the width of $\boldsymbol{A}$ and $\boldsymbol{B}$ should be compared from the two cases in Eq. (13).

$$m(\boldsymbol{A}) \leq m(\boldsymbol{B}) \tag{12}$$

$$\begin{cases} \text{Case 1}: \ w(\boldsymbol{A}) \leq w(\boldsymbol{B}) \\ \text{Case 2}: \ w(\boldsymbol{A}) > w(\boldsymbol{B}) \end{cases} \tag{13}$$

In Case 1, interval number $\boldsymbol{A}$ has less midpoint and width than $\boldsymbol{B}$. Thus, it is obvious that $\boldsymbol{A}$ is superior to $\boldsymbol{B}$.

In Case 2, interval number $\boldsymbol{A}$ has a less midpoint with greater width than $\boldsymbol{B}$. It is difficult to judge which one is preferred. The tradeoff between midpoint and width by the decision maker (DM) is needed for this case. A fuzzy set B' is defined as:

$$B' = \{(\boldsymbol{A}, \boldsymbol{B}) \mid m(\boldsymbol{A}) \leq m(\boldsymbol{B}), w(\boldsymbol{A}) > w(\boldsymbol{B})\} \tag{14}$$

The probability $P_{B'}(\boldsymbol{A})$ represents the preference degree between $\boldsymbol{A}$ and $\boldsymbol{B}$, which can be expressed by (Sengupta and Pal, 2000):

$$P_{B'}(\boldsymbol{A}) = \begin{cases} 1 & \text{if } m(\boldsymbol{A}) = m(\boldsymbol{B}) \\ \dfrac{a^{\mathrm{R}} - b^{\mathrm{R}}}{w(\boldsymbol{A}) - w(\boldsymbol{B})} & \text{if } m(\boldsymbol{A}) \leq m(\boldsymbol{B}) \leq a^{\mathrm{R}} - w(\boldsymbol{B}) \\ 0 & \text{otherwise} \end{cases} \tag{15}$$

If $P_{B'}(\boldsymbol{A}) = 1$, interval $\boldsymbol{A}$ is completely rejected. If $P_{B'}(\boldsymbol{A}) = 0$, interval $\boldsymbol{A}$ is completely accepted. If $P_{B'}(\boldsymbol{A})$ is between 0 and 1, $P_{B'}(\boldsymbol{A})$ represents the possibility degree of rejecting $\boldsymbol{A}$ and accepting $\boldsymbol{B}$.

A threshold ξ is given to represent the DM's risk tolerance to the uncertainty level of interval numbers. Then the order relation of interval numbers can be defined as follows: if $P_{B'}(\boldsymbol{A}) > \xi$, interval $\boldsymbol{B}$ is accepted and $\boldsymbol{A}$ is rejected; if $P_{B'}(\boldsymbol{A}) < \xi$, $\boldsymbol{A}$ is superior to B; if $P_{B'}(\boldsymbol{A}) = \xi$, interval $\boldsymbol{A}$ and $\boldsymbol{B}$ are equivalent. It can be seen that:

(1) if ξ is set to 0, any interval $\boldsymbol{B}$ with a smaller width will be preferred to interval $\boldsymbol{A}$. The DM only considers the interval width and has the minimal tolerance to the uncertainty level of interval numbers.

(2) if ξ is equal to 1, any interval $\boldsymbol{A}$ with a less midpoint will be superior to interval $\boldsymbol{B}$. The DM only considers the interval midpoint and has the greatest tolerance to the interval uncertainty.

(3) The DM pays more attention to the interval midpoint rather than the interval width with the increasing of the threshold ξ.

As a result, the interval comparison between $\boldsymbol{A}$ and $\boldsymbol{B}$ can be turned into the comparison of $P_{B'}(\boldsymbol{A})$ and ξ. Combined Eqs. (3) and (15), $P_{B'}(\boldsymbol{A}) < \xi$ can be converted into Eq. (16) as below.

$$m(\boldsymbol{A}) - (\xi - 1) \cdot w(\boldsymbol{A}) < m(\boldsymbol{B}) - (\xi - 1) \cdot w(\boldsymbol{B}) \tag{16}$$

If Eq. (16) is true, the following three situations can be proved.

(1) if $w(\boldsymbol{A}) > w(\boldsymbol{B})$, then $m(\boldsymbol{A}) < m(\boldsymbol{B})$ and $P_{B'}(\boldsymbol{A}) < \xi$. The interval $\boldsymbol{A}$ is preferred to $\boldsymbol{B}$.

(2) if $w(\boldsymbol{A}) \leq w(\boldsymbol{B})$ and $m(\boldsymbol{A}) \leq m(\boldsymbol{B})$, this situation is Case 1 in Eq. (13). $\boldsymbol{A}$ is preferred to $\boldsymbol{B}$.

(3) if $w(\boldsymbol{A}) < w(\boldsymbol{B})$ and $m(\boldsymbol{A}) > m(\boldsymbol{B})$, the possibility degree of accepting $\boldsymbol{A}$ can be defined as follows:

$$P_{A'}(\boldsymbol{B}) = \begin{cases} 1 & \text{if } m(\boldsymbol{B}) = m(\boldsymbol{A}) \\ \dfrac{b^{\mathrm{R}} - a^{\mathrm{R}}}{w(\boldsymbol{B}) - w(\boldsymbol{A})} & \text{if } m(\boldsymbol{B}) \leq m(\boldsymbol{A}) \leq b^{\mathrm{R}} - w(\boldsymbol{A}) \\ 0 & \text{otherwise} \end{cases} \tag{17}$$

Eq. (16) can be converted into Eq. (18) as below:

$$\frac{m(\boldsymbol{B}) + w(\boldsymbol{B}) - m(\boldsymbol{A}) - w(\boldsymbol{A})}{w(\boldsymbol{B}) - w(\boldsymbol{A})} > \xi \tag{18}$$

It is obvious that Eq. (18) is equivalent to $P_{A'}(\boldsymbol{B}) > \xi$, which indicates that $\boldsymbol{A}$ is preferred to $\boldsymbol{B}$. From the above analysis, we can draw the conclusion that Eq. (16) is the necessary and sufficient condition for judging $\boldsymbol{A}$ is preferred to $\boldsymbol{B}$.

3. Problem formulation

3.1. Natural gas system modeling

The natural gas system is composed of gas wells, gas pipelines, gas storage facilities and different kinds of gas loads.

The upper and lower limits of gas wells can be represented as:

$$Q_{s,\min} \leq Q_{s,t} \leq Q_{s,\max} \tag{19}$$

where $Q_{s,\min}$ and $Q_{s,\max}$ are the minimum and maximum gas supply flow of gas well s, respectively, $Q_{s,t}$ is the gas supply flow of gas well s at time period t.

The flow equation of natural gas pipeline can be expressed as:

$$\begin{aligned} q_{ij,t} &= \mathrm{sgn}(p_{i,t}, p_{j,t}) C_{ij} \sqrt{\left|p_{i,t}^2 - p_{j,t}^2\right|} \\ \mathrm{sgn}(p_{i,t}, p_{j,t}) &= \begin{cases} 1 & p_{i,t} \geq p_{j,t} \\ -1 & p_{i,t} < p_{j,t} \end{cases} \end{aligned} \tag{20}$$

$$q_{ij,t} = \left(q_{ij,t}^{\mathrm{in}} + q_{ij,t}^{\mathrm{out}}\right) \Big/ 2 \tag{21}$$

where $p_{i,t}$ and $p_{j,t}$ represent the pressures at node i and j, respectively, C_{ij} is a constant related to the temperature, length, inner diameter and compression factor of the pipeline from node i to node j, the function $\mathrm{sgn}(\cdot)$ indicates the direction of gas flow in the pipeline, $q_{ij,t}$ represents the average flow from node i to node j at hour t, $q_{ij,t}^{\mathrm{in}}$ and $q_{ij,t}^{\mathrm{out}}$ are the injection flow at node i and output flow at node j at hour t, respectively.

The node pressure is subject to the constraint below.

$$p_{i,\min} \leq p_{i,t} \leq p_{i,\max} \tag{22}$$

where $p_{i,\min}$ and $p_{i,\max}$ represent the minimum and maximum allowed pressure at node i, respectively.

For a certain pipeline, the difference between $q_{ij,t}^{\mathrm{in}}$ and $q_{ij,t}^{\mathrm{out}}$ can be stored in the pipeline, which is regarded as the line pack as follows (Zhang et al., 2019):

$$L_{ij,t} = M_{ij} p_{ij,t} \tag{23}$$

$$p_{ij,t} = \left(p_{i,t} + p_{j,t}\right) \Big/ 2 \tag{24}$$

$$L_{ij,t} = L_{ij,t-1} + q_{ij,t}^{\mathrm{in}} - q_{ij,t}^{\mathrm{out}} \tag{25}$$

where $L_{ij,t}$ and $p_{ij,t}$ represent the line pack and the average pressure in the pipeline from node i to node j at time period t, respectively, M_{ij} is a constant related to the pipeline characteristic.

Similar to the power balance in power system, the flow equilibrium equation for node j in the gas network can be expressed as:

$$\sum_{s \in j} Q_{s,t} + \sum_{i \in j} \left(q_{ij,t}^{\mathrm{out}} - q_{ji,t}^{\mathrm{in}}\right) - Q_{\mathrm{L},j,t} - \sum_{g \in j} Q_{g,t} = 0 \tag{26}$$

where $s \in j$ represents all the gas suppliers connected to node j, $i \in j$ represents all the nodes connected to node j, $g \in j$ represents all the gas-fired units connected to node j, $Q_{\mathrm{L},j,t}$ is the gas load of node j at time period t, $Q_{g,t}$ is the gas flow consumed by gas-fired units connected to node j at time period t.

If the natural gas system is in steady state without the consideration of the gas dynamic process, the following equations can be obtained.

$$q_{ij,t} = q_{ij,t}^{\mathrm{in}} = q_{ij,t}^{\mathrm{out}} \tag{27}$$

$$\sum_{s \in j} Q_{s,t} + \sum_{i \in j} \left(q_{ij,t} - q_{ji,t}\right) - Q_{\mathrm{L},j,t} - \sum_{g \in j} Q_{g,t} = 0 \tag{28}$$

3.2. Power system modeling

The relationship of the output and the gas consumption can be represented by:

$$Q_{g,t} = f_{GU}(P_{g,t}) = a_g \cdot P_{g,t}^2 + b_g \cdot P_{g,t} + c_g \tag{29}$$

where a_g, b_g and c_g are the fuel consumption coefficients of gas-fired unit g, $P_{g,t}$ represents the output power of unit g at time period t.

The generating unit constraints contain the output limits, operation ramp rate limits and minimum on/off time limits as shown in Eqs. (30)–(32).

$$P_{g,\min} I_{g,t} \le P_{g,t} \le P_{g,\max} I_{g,t} \tag{30}$$

$$-DR_g \le P_{g,t} - P_{g,t-1} \le UR_g \tag{31}$$

$$\begin{cases} (t_{g,t-1}^{\text{on}} - T_g^{\text{on}})(I_{g,t-1} - I_{g,t}) \ge 0 \\ (t_{g,t-1}^{\text{off}} - T_g^{\text{off}})(I_{g,t} - I_{g,t-1}) \ge 0 \end{cases} \tag{32}$$

where $P_{g,\min}$ and $P_{g,\max}$ represent the minimum and maximum output power of unit g, respectively; DR_g and UR_g are the ramp-down rate and ramp-up rate of unit g, respectively; T_g^{on} and T_g^{off} are the minimum on and off time of unit g, respectively; $t_{g,t-1}^{\text{on}}$ and $t_{g,t-1}^{\text{off}}$ represent the on and off time of unit g until the time period $t-1$, respectively; $I_{g,t}$ is the on/off state of unit g at time period t.

The injection power of bus b can be expressed by:

$$P_{b,t}^{\text{inj}} = P_{g,t} + \sum_{w \in b}(W_{w,t} - W_{\text{cur},t}) + P_{\text{L},b,t} - P_{\text{cur},b,t} \tag{33}$$

where $P_{b,t}^{\text{inj}}$ represents the injection power of bus b at time period t, $w \in b$ represents all the wind farms connected to bus b, $W_{w,t}$ and $W_{\text{cur},t}$ represent the actual wind power and curtailed wind power of wind farm w at hour t, respectively, $P_{\text{L},b,t}$ and $P_{\text{cur},b,t}$ are the electric load and the unserved load of bus b at hour t, respectively.

The power transmission constraint can be expressed by:

$$-f_{l,\max} \le \sum_{b=1}^{N_b} k_{l,b} P_{b,t}^{\text{inj}} \le f_{l,\max} \tag{34}$$

where $f_{l,\max}$ represents the maximum transmission power of branch l, $k_{l,b}$ is the sensitivity factor of branch l to bus b, N_b is the number of buses.

The power balance equation is as follows:

$$\sum_{g \in GU \bigcup TU} P_{g,t} + \sum_{w \in WF}(W_{w,t} - W_{\text{cur},t}) = P_{\text{L},t} - P_{\text{cur},t} \tag{35}$$

$$P_{\text{L},t} = \sum_{b=1}^{N_b} P_{\text{L},b,t}, \quad P_{\text{cur},t} = \sum_{b=1}^{N_b} P_{\text{cur},b,t} \tag{36}$$

where $P_{\text{L},t}$ and $P_{\text{cur},t}$ represent the total electric load and unserved load in the power network at time period t, respectively, GU represents the set of gas-fired units, TU represents the set of thermal units, and WF is the set of wind farms.

3.3. Demand response management

The price elasticity of residential gas demand is not easy to obtain, the gas demand response (DR) model is established from the perspective of consumer psychology. As a new pricing mechanism, the peak–valley time-of-use pricing of natural gas will produce external environmental stimulation to the consumers' gas consumption behavior. The "price sensitivity" is introduced in this study to measure the residents' response to this mechanism (Wardono and Fathi, 2004). According to the relative income theory by Duesenberry (Pinedo, 2007), the expenditure on natural gas by residents with higher income accounts for a smaller proportion of their total expenditure on household consumption. As a result, the residents with higher income are less sensitive to the price of natural gas. Based on the above analysis, the price sensitivity function of residential gas demand is as follows (Zhang and Zhang, 2007):

$$PS_r = \alpha^{|p_{TOU} - p_P|} + |p_{TOU} - p_P| \times \frac{C_r}{I_r} \tag{37}$$

where C_r represents the expenditure on gas consumption by resident r, C_r represents the disposable income of resident r, p_{TOU} is the real time gas price of residents, p_P is the gas price at normal periods, and α indicates the gas price elasticity of residents.

Then the natural gas demand response function of resident r at the peak and valley periods can be obtained by:

$$d_{r,t} = \begin{cases} d_{r,t}^0 \times [2 - \alpha^{p_F - p_P} - (p_F - p_P) \times C_r / I_r] & t \in t_F \\ d_{r,t}^0 \times [\alpha^{p_P - p_G} + (p_P - p_G) \times C_r / I_r] & t \in t_G \end{cases} \tag{38}$$

$$Q_{\text{L},j,t}^* = \sum_{r \in j} d_{r,t} \tag{39}$$

where $d_{r,t}^0$ represents the original gas consumption of resident r at time period t, $d_{r,t}$ represents the adjusted gas consumption, p_F and p_G are the gas price at peak periods and valley periods, respectively, t_F and t_G represent the peak period set and valley period set, respectively, $Q_{\text{L},j,t}^*$ is the total residential gas load of node j at time period t after applying gas demand response.

For the electric load, the demand shifting strategy is considered in this study. For example, it is beneficial to shift the residential power load from the peak time periods to the valley time periods with abundant wind power output. The load demand after adopting the demand shifting strategy can be expressed by (Alham et al., 2016):

$$P_{\text{L},b,t}^* = P_{\text{L},b,t} + P_{\text{up},b,t} - P_{\text{dn},b,t} \tag{40}$$

where $P_{\text{L},b,t}^*$ represents the load demand adopting the demand shift strategy of bus b at hour t, $P_{\text{up},b,t}$ and $P_{\text{dn},b,t}$ are the upward/downward load increment of bus b at hour t.

The load shift during the whole scheduling period is subject to the following constraints.

$$\sum_{t=1}^{T} P_{\text{up},b,t} - \sum_{t=1}^{T} P_{\text{dn},b,t} = 0, \quad b \in N_b \tag{41}$$

$$\begin{cases} 0 \le P_{\text{up},b,t} \le \lambda_{\text{up}} \times P_{\text{L},b,t} \\ 0 \le P_{\text{dn},b,t} \le \lambda_{\text{dn}} \times P_{\text{L},b,t} \end{cases}, \quad b \in N_b \tag{42}$$

where λ_{up} and λ_{dn} are the maximum percentage of the upward and downward shift load increment in the original load demand, respectively.

4. Coordination scheduling of integrated energy system

4.1. Deterministic optimization model

The optimization objective is given as follows:

$$\min \left\{ \sum_t \left[\begin{array}{l} \sum_{g \in GU} \rho_g Q_{g,t} + \sum_{g \in TU} f_{TU}(P_{g,t}) + \\ \sum_{g \in GU \bigcup TU} CS_{g,t} + \sum_{w \in WF} \rho_w W_{\text{cur},t} + \rho_e P_{\text{cur},t} \end{array} \right] \right\} \tag{43}$$

where ρ_g is the contract price of natural gas for the gas-fired units, f_{TU} represents the generation cost function of the thermal

units, $CS_{g,t}$ is the startup cost of unit g at time period t, ρ_w and ρ_e are the penalty factors for the curtailed wind power and the unserved electric load, respectively.

As shown in Fig. 1, the coordination scheduling problem is decomposed into the mix-integer linear programming (MILP) problem for power system and the natural gas system subproblem. The MILP problem solves the day-ahead unit commitment and dispatch plan while meeting the power system constraints. Then the subproblem would check the gas network feasibility after the gas-fired units is determined. If any gas network constraint is violated, the natural gas usage constraints will be formed and fed back to the MILP problem to modify the day-ahead dispatch plan. The above process will be repeated until the gas network constraints are satisfied.

Since the simulations in this study are implemented using the CPLEX solver, the constraints should be linear. Thus, the nonlinear equations (20) and (29) should be linearized (Carrión and Arroyo, 2006), the detailed linearization methods of which can be found in Appendix.

4.2. Interval optimization model

4.2.1. Interval variable description

The interval forecasting results of wind power are easy to acquire in practice. Hence, the interval number noted as $\boldsymbol{W}_{w,t}$ is used to handle wind power uncertainty as follows:

$$\boldsymbol{W}_{w,t} = [W^{\mathrm{L}}_{w,t}, W^{\mathrm{R}}_{w,t}] = \{W_{w,t} \mid W^{\mathrm{L}}_{w,t} \le W_{w,t} \le W^{\mathrm{R}}_{w,t}\} \tag{44}$$

where $W^{\mathrm{L}}_{w,t}$ and $W^{\mathrm{R}}_{w,t}$ represent the lower and upper boundaries of wind power prediction of wind farm w at hour t.

To deal with wind power uncertainty, the output of units, the curtailed wind power, the unserved electric load will change within a certain range. In addition, the corresponding gas consumption of the gas-fired units will vary in a certain range.

$$\boldsymbol{P}_{g,t} = [P^{\mathrm{L}}_{g,t}, P^{\mathrm{R}}_{g,t}] = \{P_{g,t} \mid P^{\mathrm{L}}_{g,t} \le P_{g,t} \le P^{\mathrm{R}}_{g,t}\} \tag{45}$$

$$\boldsymbol{W}_{\mathrm{cur},t} = [W^{\mathrm{L}}_{\mathrm{cur},t}, W^{\mathrm{R}}_{\mathrm{cur},t}] = \{W_{\mathrm{cur},t} \mid W^{\mathrm{L}}_{\mathrm{cur},t} \le W_{\mathrm{cur},t} \le W^{\mathrm{R}}_{\mathrm{cur},t}\} \tag{46}$$

$$\boldsymbol{P}_{\mathrm{cur},t} = [P^{\mathrm{L}}_{\mathrm{cur},t}, P^{\mathrm{R}}_{\mathrm{cur},t}] = \{P_{\mathrm{cur},t} \mid P^{\mathrm{L}}_{\mathrm{cur},t} \le P_{\mathrm{cur},t} \le P^{\mathrm{R}}_{\mathrm{cur},t}\} \tag{47}$$

where $P^{\mathrm{L}}_{g,t}$ and $P^{\mathrm{R}}_{g,t}$ are the left and right limits of power output by unit g at hour t, $W^{\mathrm{L}}_{\mathrm{cur},t}$ and $W^{\mathrm{R}}_{\mathrm{cur},t}$ are the left and right limits of wind curtailment at hour t, $P^{\mathrm{L}}_{\mathrm{cur},t}$ and $P^{\mathrm{R}}_{\mathrm{cur},t}$ are the left and right limits of unserved power load at hour t

4.2.2. The constraints transformation for interval optimization

The power system constraints containing the interval variables are expressed as:

$$P_{g,\min} \le [P^{\mathrm{L}}_{g,t}, P^{\mathrm{R}}_{g,t}] \le P_{g,\max} \tag{48}$$

$$-DR_g \le [P^{\mathrm{L}}_{g,t}, P^{\mathrm{R}}_{g,t}] - [P^{\mathrm{L}}_{g,t-1}, P^{\mathrm{R}}_{g,t-1}] \le UR_g \tag{49}$$

$$0 \le [W^{\mathrm{L}}_{\mathrm{cur},t}, W^{\mathrm{R}}_{\mathrm{cur},t}] \le [W^{\mathrm{L}}_{w,t}, W^{\mathrm{R}}_{w,t}] \tag{50}$$

$$0 \le [P^{\mathrm{L}}_{\mathrm{cur},t}, P^{\mathrm{R}}_{\mathrm{cur},t}] \le P_{\mathrm{L},t} \tag{51}$$

As the minimization problem has been discussed in Section 2.2, the maximization problem in (48) can be transformed into a minimization problem by multiplying by -1 on both sides. Thus, (48) can be converted into (52) and (53) as follows:

$$[P^{\mathrm{L}}_{g,t}, P^{\mathrm{R}}_{g,t}] \le P_{g,\max} \tag{52}$$

$$(-1)\cdot[P^{\mathrm{L}}_{g,t}, P^{\mathrm{R}}_{g,t}] \le -P_{g,\min} \tag{53}$$

Then (52) and (53) can further be converted into the deterministic constraints by introducing the order relation of interval numbers as shown in (54) and (55).

$$(P^{\mathrm{L}}_{g,t} + P^{\mathrm{R}}_{g,t})/2 - (\xi_g - 1)\cdot(P^{\mathrm{R}}_{g,t} - P^{\mathrm{L}}_{g,t})/2 \le P_{g,\max} \tag{54}$$

$$(P^{\mathrm{L}}_{g,t} + P^{\mathrm{R}}_{g,t})/2 + (\xi_g - 1)\cdot(P^{\mathrm{R}}_{g,t} - P^{\mathrm{L}}_{g,t})/2 \ge P_{g,\min} \tag{55}$$

where ξ_g represents the degree of pessimism for the output power by unit g. It is set to 0 to prevent the constraint violation.

Similarly, constraint (49) can be converted into (56) and (57) by combining the order relation and basic arithmetic of interval numbers.

$$(P^{\mathrm{L}}_{g,t} + P^{\mathrm{R}}_{g,t} - P^{\mathrm{L}}_{g,t-1} - P^{\mathrm{R}}_{g,t-1})/2 - (\xi_r - 1)\cdot(P^{\mathrm{R}}_{g,t} + P^{\mathrm{R}}_{g,t-1} - P^{\mathrm{L}}_{g,t} - P^{\mathrm{L}}_{g,t-1})/2 \le UR_g \tag{56}$$

$$(P^{\mathrm{L}}_{g,t} + P^{\mathrm{R}}_{g,t} - P^{\mathrm{L}}_{g,t-1} - P^{\mathrm{R}}_{g,t-1})/2 + (\xi_r - 1)\cdot(P^{\mathrm{R}}_{g,t} + P^{\mathrm{R}}_{g,t-1} - P^{\mathrm{L}}_{g,t} - P^{\mathrm{L}}_{g,t-1})/2 \ge -DR_g \tag{57}$$

where ξ_r represents the degree of pessimism for the output power adjustment between the adjacent periods and is set to 0.7.

In addition, Eqs. (50) and (51) can be converted into the deterministic constraints in the same way, which is not described to save space.

On the other hand, the equality constraints (29) and (35) containing interval variables can be handled as follows:

$$\begin{cases} Q^{\mathrm{L}}_{g,t} = f_{GU}(P^{\mathrm{L}}_{g,t}), \quad Q^{\mathrm{R}}_{g,t} = f_{GU}(P^{\mathrm{R}}_{g,t}), \ \boldsymbol{Q}_{g,t} = [Q^{\mathrm{L}}_{g,t}, Q^{\mathrm{R}}_{g,t}], \ g \in GU \\ C^{\mathrm{L}}_{g,t} = f_{TU}(P^{\mathrm{L}}_{g,t}), \quad C^{\mathrm{R}}_{g,t} = f_{TU}(P^{\mathrm{R}}_{g,t}), \ \boldsymbol{C}_{g,t} = [C^{\mathrm{L}}_{g,t}, C^{\mathrm{R}}_{g,t}], \ g \in TU \end{cases} \tag{58}$$

$$\sum_{g\in GU\bigcup TU} \boldsymbol{P}_{g,t} + \sum_{w\in WF} (\boldsymbol{W}_{w,t} - \boldsymbol{W}_{\mathrm{cur},t}) = P_{\mathrm{L},t} - \boldsymbol{P}_{\mathrm{cur},t} \tag{59}$$

where $C^{\mathrm{L}}_{g,t}$ and $C^{\mathrm{R}}_{g,t}$ denote the left/right limits of generating cost for thermal unit g.

As there exist several interval variables in (59), it cannot be easily converted into deterministic constraints. It should be transformed according to the possible situations.

For the unserved load, the right limit of $\boldsymbol{P}_{\mathrm{cur},t}$ can be obtained when the generating units produce the maximum power and wind farm has the minimum output as shown in Eq. (60), where the function 'max' is used to guarantee the unserved load is non-negative. Similarly, the left limit of $\boldsymbol{P}_{\mathrm{cur},t}$ can be obtained as shown in Eq. (61).

$$P^{\mathrm{R}}_{\mathrm{cur},t} = \max(P_{\mathrm{L},t} - \sum_{w\in WF} W^{\mathrm{L}}_{w,t} - \sum_{g\in GU\bigcup TU} P^{\mathrm{R}}_{g,t},\ 0) \tag{60}$$

$$P^{\mathrm{L}}_{\mathrm{cur},t} = \max(P_{\mathrm{L},t} - \sum_{w\in WF} W^{\mathrm{R}}_{w,t} - \sum_{g\in GU\bigcup TU} P^{\mathrm{R}}_{g,t},\ 0) \tag{61}$$

For the curtailed wind power, the right limit can be acquired if the units achieve the lower limit and the wind farms reach the upper limit; the left limit can be obtained if the generating units and wind farms achieve the lower limit simultaneously.

$$\sum_{w\in WF} W^{\mathrm{R}}_{\mathrm{cur},t} = \max(\sum_{w\in WF} W^{\mathrm{R}}_{w,t} + \sum_{g\in GU\bigcup TU} P^{\mathrm{L}}_{g,t} - P_{\mathrm{L},t},\ 0) \tag{62}$$

$$\sum_{w\in WF} W^{\mathrm{L}}_{\mathrm{cur},t} = \max(\sum_{w\in WF} W^{\mathrm{L}}_{w,t} + \sum_{g\in GU\bigcup TU} P^{\mathrm{L}}_{g,t} - P_{\mathrm{L},t},\ 0) \tag{63}$$

It can be seen from Eq. (60) that if the right limit of the unserved load is positive, the Eq. (64) is always true, and it can be deduced from Eq. (62) that if the right limit of the curtailed wind power is positive, the Eq. (65) is true.

$$P^{\mathrm{R}}_{\mathrm{cur},t} = P_{\mathrm{L},t} - \sum_{w\in WF} W^{\mathrm{L}}_{w,t} - \sum_{g\in GU\bigcup TU} P^{\mathrm{R}}_{g,t} \quad \text{if } P^{\mathrm{R}}_{\mathrm{cur},t} > 0 \tag{64}$$

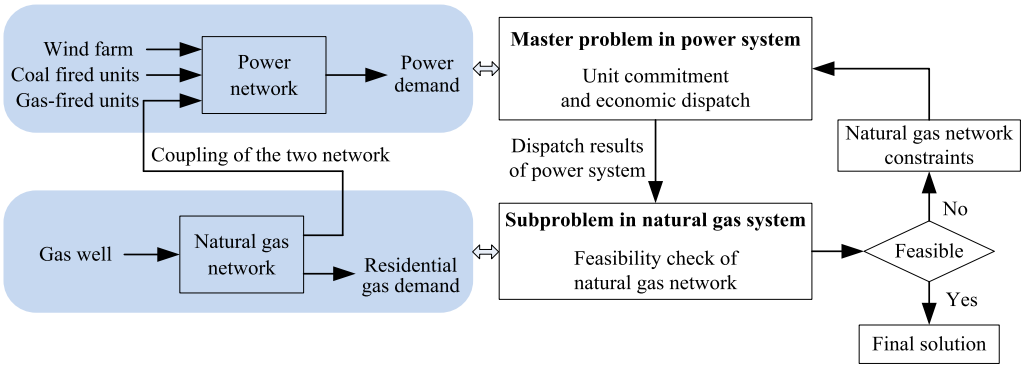

Fig. 1. Master-subproblem framework for the coordination scheduling.

$$\sum_{w\in WF} W^{\mathrm{R}}_{\mathrm{cur},t} = \sum_{w\in WF} W^{\mathrm{R}}_{w,t} + \sum_{g\in GU\bigcup TU} P^{\mathrm{L}}_{g,t} - P_{\mathrm{L},t} \quad \text{if} \sum_{w\in WF} W^{\mathrm{R}}_{\mathrm{cur},t} > 0 \tag{65}$$

Additionally, the gas flow in the pipelines and the pressure at the gas nodes should be considered as interval numbers. We should check natural gas network operation feasibility when using the interval-based optimization model. The degrees of pessimism for the constraints in natural gas system are set to 0 to prevent the constraint violation.

4.2.3. The objective function transformation

The objective function containing the interval variables can be expressed as:

$$\boldsymbol{F} = \langle m(\boldsymbol{F}),\ w(\boldsymbol{F})\rangle \tag{66}$$

where $m(\boldsymbol{F})$ and $w(\boldsymbol{F})$ represent the midpoint and width of the objective, respectively.

Then the minimization for interval optimization is given as:

$$\begin{aligned}
&\min\ m(\boldsymbol{F}) - (\xi_f - 1)\cdot w(\boldsymbol{F})\\
&= \sum_t [\sum_{g\in GU} \rho_g m(\boldsymbol{Q}_{g,t}) - \sum_{g\in GU} \rho_g(\xi_f - 1) w(\boldsymbol{Q}_{g,t}) + \sum_{g\in TU} m(\boldsymbol{C}_{g,t})\\
&- \sum_{g\in TU} (\xi_f - 1) w(\boldsymbol{C}_{g,t}) + \sum_{w\in WF} \rho_w m(\boldsymbol{W}_{\mathrm{cur},t})\\
&- \sum_{w\in WF} \rho_w (\xi_f - 1) w(\boldsymbol{W}_{\mathrm{cur},t})\\
&+ \rho_e m(\boldsymbol{P}_{\mathrm{cur},t}) - (\xi_f - 1) w(\boldsymbol{P}_{\mathrm{cur},t}) + \sum_{g\in GU\bigcup TU} CS_{g,t}]
\end{aligned} \tag{67}$$

where ξ_f represents the degree of pessimism for the operation cost and is set to 0.5.

5. Case study

The effectiveness of proposed interval-based coordination scheduling model is evaluated on two test systems: a 6-bus power system with a 6-node natural gas system and the modified IEEE118-bus system with a 10-node natural gas system. The simulation of the above test systems is implemented in MATLAB with CPLEX solver on a PC with Intel Core i7 1.8 GHz CPU and 8 GB RAM. The absolute and relative tolerances on the gap for CPLEX are set to 10^{-6} and 10^{-4}, respectively, and the other parameters remain default.

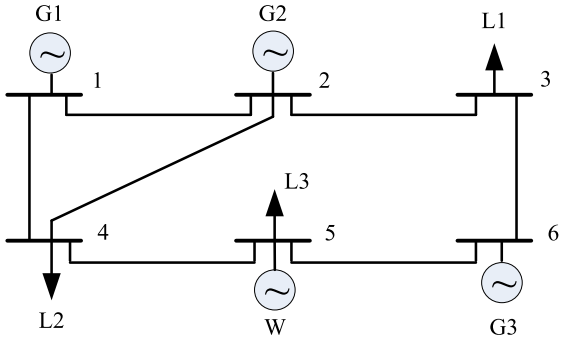

Fig. 2. 6-bus power system.

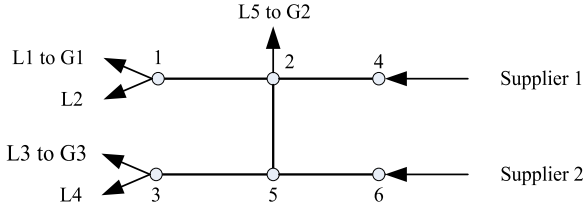

Fig. 3. 6-node natural gas system.

5.1. 6-bus power system with 6-node natural gas system

In the 6-bus power system shown in Fig. 2, three gas-fired units are located at bus 1, 2 and 6, respectively; three electric loads are at bus 3, 4 and 5, respectively, and the demand response is implemented at bus 5. The wind farm is installed at bus 5. In the 6-node natural gas system depicted in Fig. 3, two gas wells are connected to node 4 and 6; two residential gas loads are at node 1 and 3 noted as L2 and L4, which account for 2/3 and 1/3 of the residential gas demand, respectively. The parameters of the test system are given in motor.ece.iit.edu/data/Gastranssmion6_2.xlsx.

The gas price for gas-fired units is 1.4 $/MBtu (Liu et al., 2011). The residential gas price for peak, normal and valley period are 2.7 $/MBtu, 1.9 $/MBtu and 1.2 $/MBtu, respectively. The valley periods are 23:00–6:00, the normal periods are 13:00–15:00 and 20:00–22:00, the peak periods are 7:00–12:00 and 16:00–19:00. The penalty for electric load shedding and curtailed wind power are 1000 $/MW and 500 $/MW, respectively.

5.1.1. Deterministic model for the integrated system without wind farm

The following four cases are established to conduct a comparative analysis.

Table 1
Comparison of results without wind farm.

	Gas-fired unit cost ($)	Load shedding cost ($)	Startup cost ($)	Total cost ($)
Case 1	132 483	14 872	500	147 855
Case 2	119 336	0	1120	120 456
Case 3	119 333	0	620	119 953
Case 4	115 381	0	620	116 001

Case 1: The DR strategies for gas and electric loads are not considered, and the multiperiod dynamic process of natural gas system is not taken into account.
Case 2: The DR strategies are considered, but the dynamic process of natural gas system is not taken into account.
Case 3: The DR strategies are not considered, but the dynamic process of natural gas system is taken into account.
Case 4: The DR strategies and the dynamic process of natural gas system are considered.

The operation results of the above four cases are listed in Table 1.

From Table 1, it can be seen that: (a) the load shedding has occurred only in Case 1, and the unserved electric load is 14.87 MW; (b) compared with Case 1, the total cost in Case 2 with the consideration of demand response has reduced by 18.53%; (c) compared with Case 1, Case 3 considering the multiperiod dynamic process of natural gas network can not only decrease the generating cost, but also guarantee the supply of the electric load; (d) Case 4 considering the dynamic process of gas network and demand response simultaneously has achieved the minimum operating cost; (e) the master-subproblem solving framework for IES in the above cases can achieve the optimal solutions within 5 iterations.

To analyze the effect of dynamic process in natural gas network on the IES, the power output of gas-fired units in Case 1 and Case 3 are shown in Fig. 4.

From Fig. 4, it can be seen that the load shedding occurs at hours 17 and 18 in Case 1. At hour 17, G1 and G2 are dispatched at 168.4 MW and 80 MW, respectively. At hour 18, G1 and G2 are dispatched at 159.4 MW and 80 MW, respectively. In other words, the output of G1 has not achieved its maximum capacity while G2 reaches its maximum capacity. Moreover, G1 is dispatched at 181.6 MW at hour 16 and the ramp rate for G1 is 55 MW/h, which indicates that the output power of G1 is not limited by its ramp rate and maximum capacity. From the above analysis, it can be concluded that the insufficient gas acquisition for G1 is the essential reason for the electric load shedding in Case 1. In other words, considering the dynamic process of natural gas network can enhance the operation reliability and economy of the gas–electricity interconnected system.

5.1.2. Deterministic model for the integrated system with wind farm

When there not exists wind farm, the maximum output for gas-fired units G1, G2 and G3 are 220 MW, 80 MW and 20 MW, respectively. Hence, the total power system capacity is 320 MW. When the 100 MW wind farm is considered, the maximum output for G1 and G2 are decreased to 145 MW and 55 MW, respectively to keep the system installation capacity constant. The comparison of results for different cases is listed in Table 2.

From Table 2, it can be seen that: (a) compared with Case 1, Case 2 considering demand response can prominently reduce the wind curtailment and load shedding cost, and the situation is similar by the comparison of Case 3 and Case 4; (b) compared with Case 2, Case 4 decreases the gas-fired unit, curtailment and load shedding cost by 12.87%, 99.15% and 77.77%, respectively, which indicates that considering the gas dynamic process can improve the reliability of the IES and enhance wind power utilization.

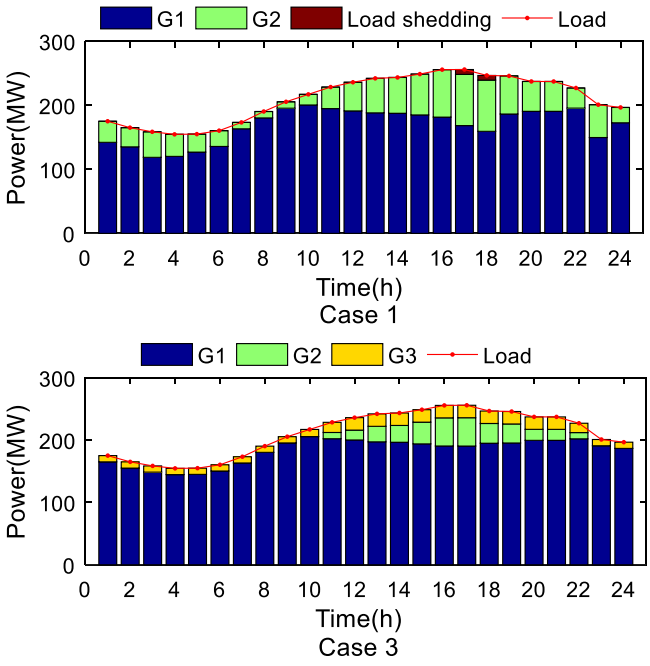

Fig. 4. The power output of gas-fired units in Case 1 and 3.

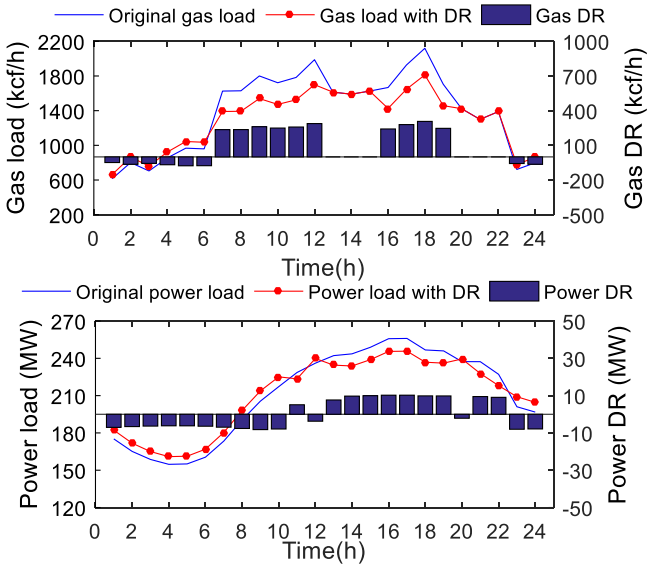

Fig. 5. The load curves with and without DR.

Table 2
Comparison of results with wind farm.

	Gas-fired unit cost ($)	Curtailment cost ($)	Load shedding cost ($)	Startup cost ($)	Total cost ($)
Case 1	106 811	124 545	95 332	500	327 188
Case 2	104 270	88 976	63 489	500	257 235
Case 3	92 229	12 770	34 584	620	140 203
Case 4	90 849	752	14 112	620	106 333

The residential gas load and power load curves with and without demand response management are shown in Fig. 5, and the dispatch results are shown in Figs. 6 and 7. It can be found that Case 4 considering the gas dynamic process and demand response strategies achieves the minimum cost of wind curtailment and load shedding.

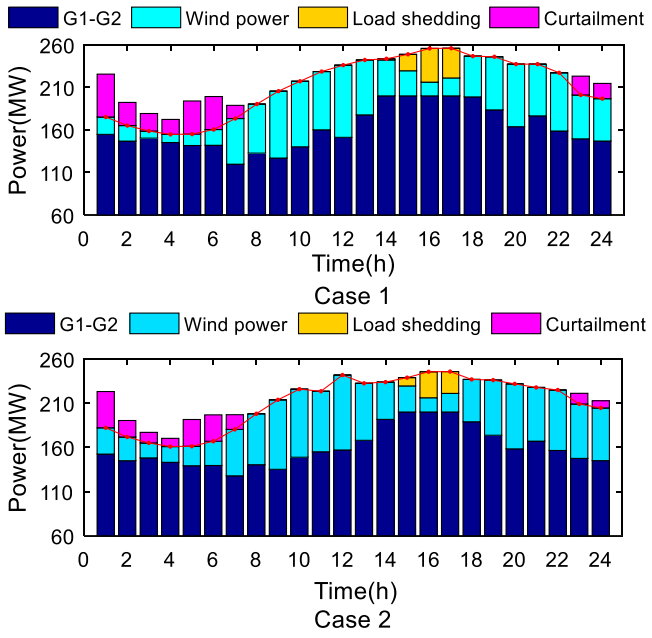

Fig. 6. The dispatch results in Case 1 and Case 2.

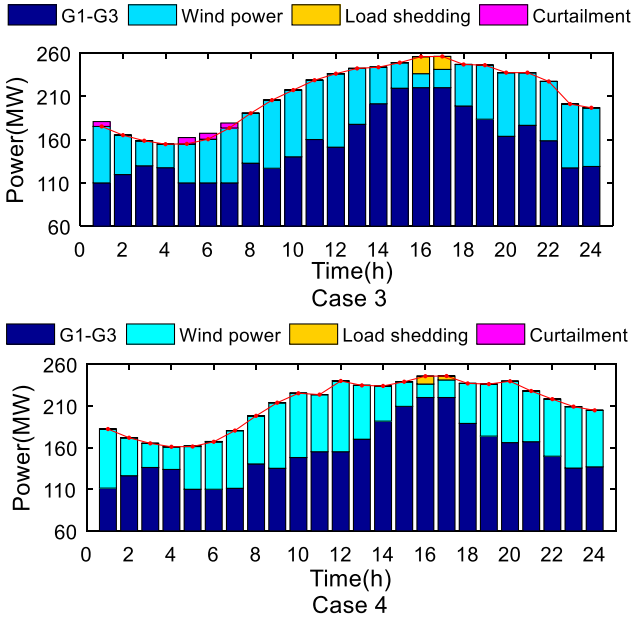

Fig. 7. The dispatch results in Case 3 and Case 4.

5.1.3. Interval model for the integrated system with wind farm

The prediction results of wind power with 10%, 20% and 30% uncertain interval are shown in Fig. 8.

To verify the performance of proposed interval optimization, the scenario-based stochastic optimization (SO) and robust optimization (RO) method are employed in this study. For SO, the scenario generation and reduction techniques (Zhang et al., 2017) are adopted to obtain the reduced scenario set containing 10 wind power scenarios. For RO, the two-stage robust optimization model is established and the column-and-constraint generation (C&CG) algorithm is used to solve the RO problem (Zeng and Zhao, 2013; He et al., 2017).

The simulation results of different methods are listed in Table 3.

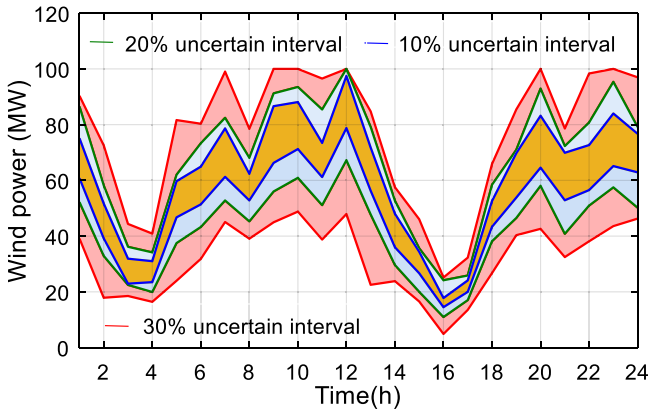

Fig. 8. The interval prediction results of wind power.

Table 3
Comparison of simulation results for Cases 3–4.

	Wind power interval (%)	Expected cost for IO ($)	Objective cost for IO ($)	Objective cost for SO($)	Objective cost for RO ($)
Case 3	10	143 197	153 725	142 889	162 197
	20	154 519	176 492	153 343	192 151
	30	180 948	221 148	159 464	244 643
Case 4	10	111 942	118 926	111 574	124 013
	20	120 175	135 729	120 114	146 373
	30	143 330	172 782	126 601	190 676

From Table 3, it can be seen that for a certain wind power interval in Case 3, the objective cost for RO is maximal and the cost for SO is minimal, and the objective cost for IO is between the above two objective values. The same situation is found in Case 4. The reason is that RO searches for the optimal operation cost under the worst wind power scenario, which results in an over-conservative scheduling strategy. On the other hand, SO attempts to minimize the expectation of operation costs for the wind power scenario sets. The computing time complexity of SO can be greatly decreased by the scenario reduction technique, but the rare extreme events could be eliminated. As a result, the strategy reliability of SO is unacceptable in the actual scheduling.

As shown in Eq. (67), the midpoint represents the expected cost and the width denotes the uncertainty degree of the solution. Considering the midpoint and width of the operation cost, the proposed IO method intends to find a solution with minimum midpoint as well as width. It can be seen the solution of IO can improve the economic performance of RO and enhance the reliability of SO simultaneously. In addition, the expected cost for IO has greatly increased as the wind power interval gets wide.

The cost compositions and its interval at each hour for IO with 10% uncertain wind power are shown in Fig. 9. Moreover, the output by gas-fired units and the power imbalance with 10%, 20% and 30% uncertain wind power are illustrated in Figs. 10–12, respectively.

Fig. 9 shows that Case 4 considering DR can remarkably decrease the curtailment and load shedding costs compared to Case 3. For Case 4, it can be seen that the wind curtailment has happened at hours 1, 6, 7 and 8 when wind power is in peak period and power load demand is in low period. On the other hand, the load shedding has occurred at hours 16 and 17 when wind power is in low period and load demand is in peak period.

From Figs. 10–12, it can be found that the output interval of gas-fired units significantly gets larger as wind power uncertainty increases, and the amount of wind curtailment and load shedding have increased in the mean while.

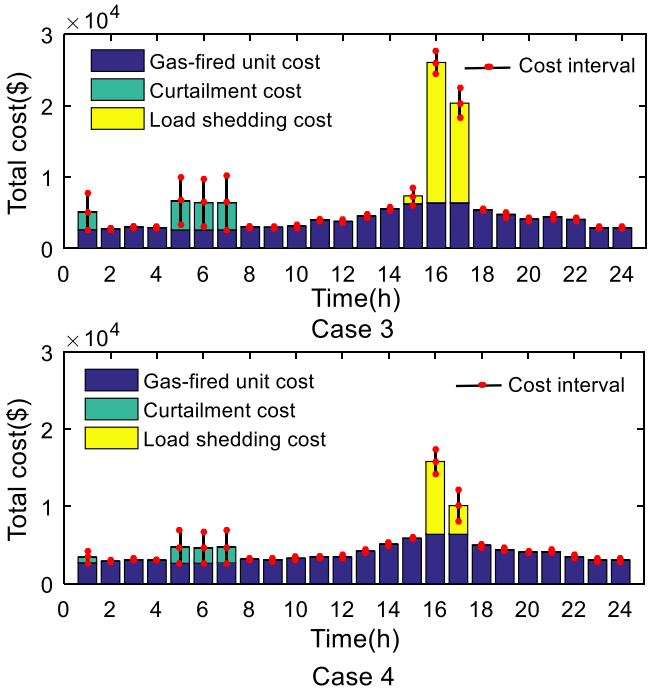

Fig. 9. The cost compositions and interval at each hour with 10% uncertain wind power.

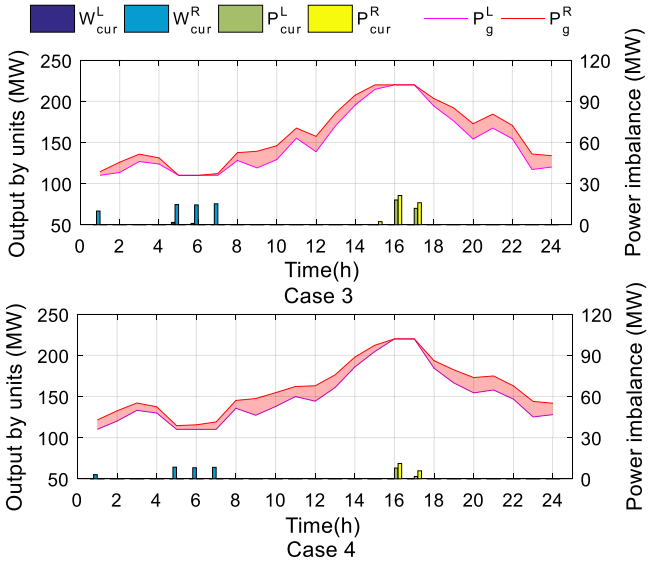

Fig. 10. The dispatch results in power system with 10% uncertain wind power.

To investigate the effect of wind farm installed capacity, the 80 MW wind farm is considered. Then the maximum output power of G1, G2 and G3 are set to 160 MW, 60 MW and 20 MW, respectively to keep system installation capacity constant. Similarly, when the wind farm capacity is set to 60 MW, the maximum output of G1, G2 and G3 are 180 MW, 60 MW and 20 MW, respectively. The total cost interval values with different wind farm capacity are listed in Tables 4 and 5, respectively.

The generating costs with different wind farm capacity and wind power uncertainty are shown in Fig. 13, and the penalty costs are shown in Fig. 14.

Combined Figs. 13 and 14, it can be seen that: (a) for a certain case, the larger the wind farm capacity is, the less the generating cost is but the more the penalty cost is; (b) compared

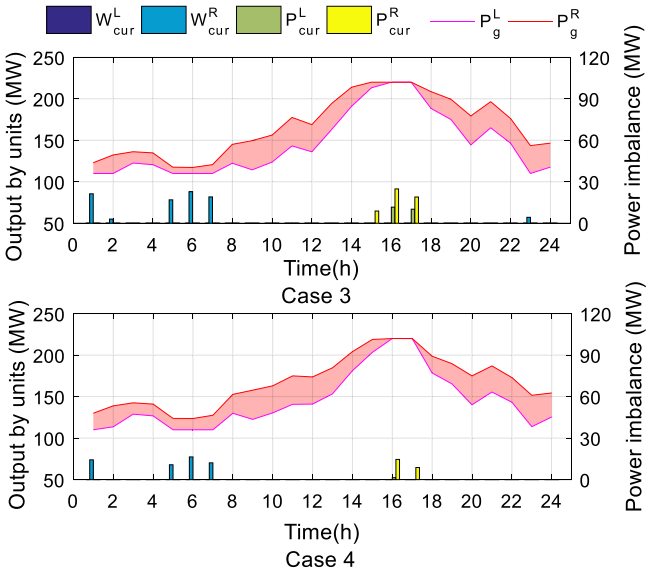

Fig. 11. The dispatch results in power system with 20% uncertain wind power.

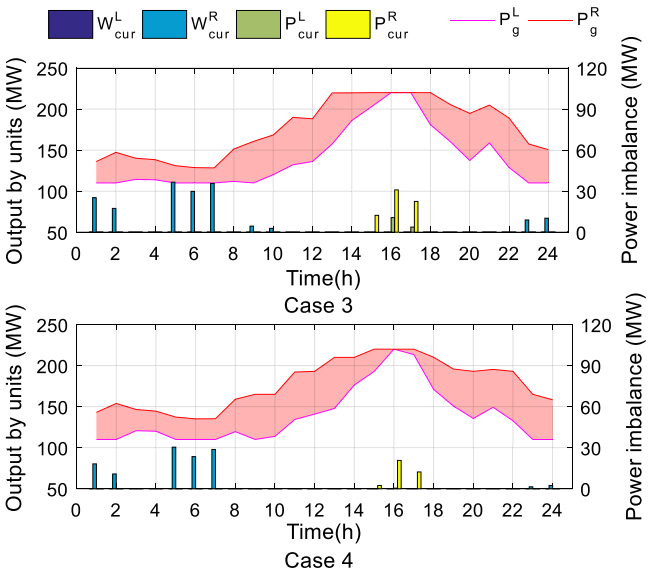

Fig. 12. The dispatch results in power system with 30% uncertain wind power.

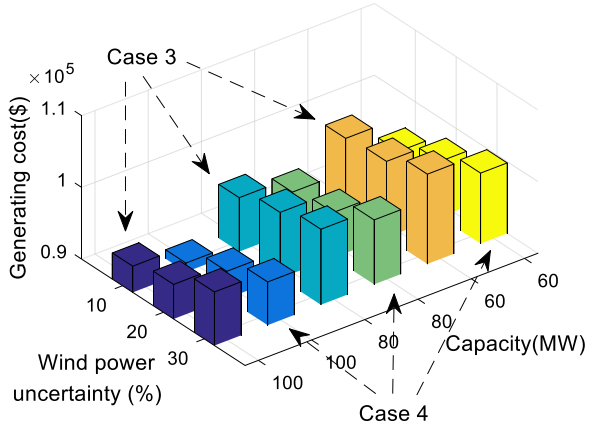

Fig. 13. The generating costs with different wind farm capacity and wind power uncertainty.

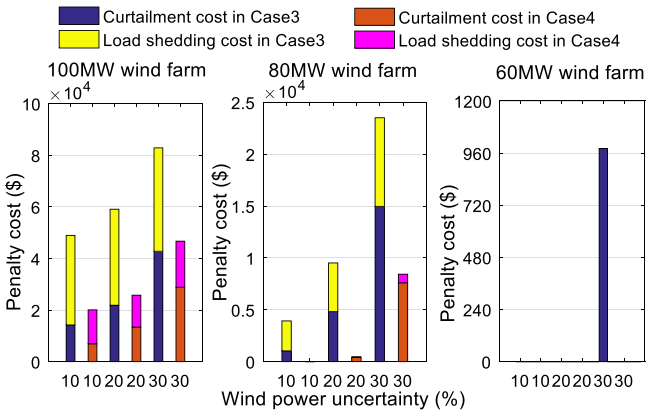

Fig. 14. The penalty costs with different wind farm capacity and wind power uncertainty.

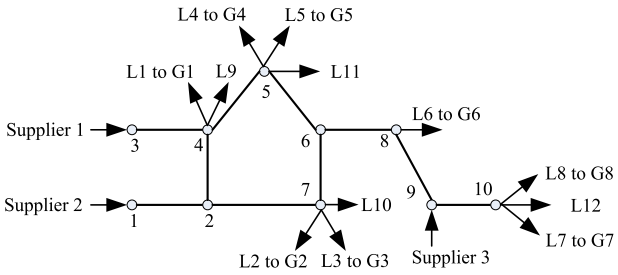

Fig. 15. 10-node natural gas system.

with Case 3, Case 4 considering demand side management can reduce the generating cost, curtailment cost and load shedding cost simultaneously.

5.2. IEEE 118-bus system with 10-node natural gas system

To verify the practicability of the proposed interval model, the modified IEEE 118-bus system interconnected with 10-node natural gas system is built in this section. The operation parameters of the test coupled system are given in motor.ece.iit.edu/data/Gastranssmion_118_10_1.xlsx. The total generation capacity of the power system is 7095 MW. As shown in Fig. 15, L9 to L12 are residential gas loads, which account for 20%, 30%, 30% and 20% of the total residential gas load, respectively.

5.2.1. Deterministic model for the integrated system

The dynamic process of natural gas system is always considered in the following simulations, and the four cases below are built to conduct a comparative analysis.

Case 1: The wind farms are not installed and the DR strategies are not considered.

Case 2: The wind farms are not installed, but the DR strategies are considered.

Case 3: The wind farms are installed, but the DR strategies are not considered.

Case 4: The wind farms are installed and the DR strategies are considered.

In the above cases, the power demand response is implemented at bus 7, 11, 14, 20, 24, 26, 39, 44, 49, 59, 61 and 68. The gas demand response is applied at node 4, 5, 7 and 10 in the gas network. Two 400 MW wind farms are installed at bus 17 and 65, respectively. To retain the total capacity of power system constant, we have reduced the capacity of units as follows: the generating capacities of the units noted as G10, G11, G27, G28, G29, G36, G39, G43, G44 and G45 are decreased to 220 MW, 270 MW, 340 MW, 340 MW, 220 MW, 220 MW, 220 MW, 220 MW,220 MW, 220 MW, respectively.

The simulation results are listed in Table 4.

From Table 4, it can be seen that compared to Case 1, Case 2 has saved the operation cost by 6844 $ while Case 4 has reduced the total cost by 9082 $ compared to Case 3. The above simulation results demonstrate that DR is an effective measure to enhance system operation economics.

Table 4
Simulation results for the deterministic model.

	Gas-fired unit cost ($)	Thermal unit cost ($)	Total cost ($)
Case 1	221 747	1 564 546	1 786 293
Case 2	217 591	1 561 858	1 779 449
Case 3	195 966	1 403 198	1 599 164
Case 4	190 052	1 400 030	1 590 082

Table 5
Comparison of simulation results for Cases 3–4.

	Wind power interval (%)	Expected cost for IO ($)	Objective cost for IO ($)	Objective cost for SO ($)	Objective cost for RO ($)
Case 3	10	1 523 498	1 535 955	1 523 625	1 538 376
	20	1 528 416	1 553 121	1 527 270	1 556 747
	30	1 533 871	1 576 289	1 531 509	1 584 499
Case 4	10	1 510 628	1 522 780	1 510 672	1 525 074
	20	1 515 249	1 539 353	1 514 213	1 542 539
	30	1 519 006	1 560 638	1 517 769	1 568 014

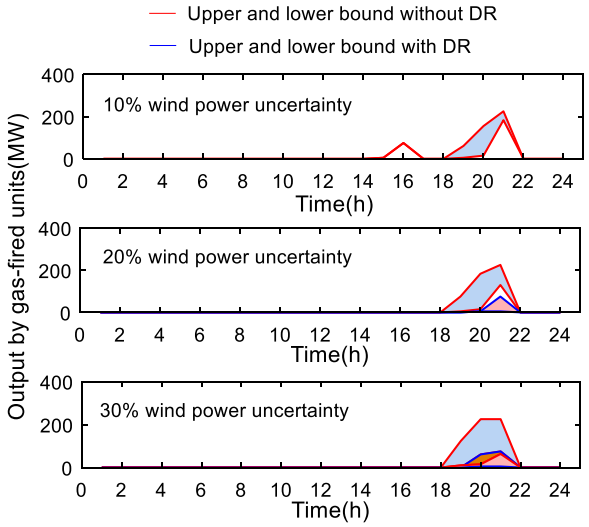

Fig. 16. The output interval of gas-fired units.

5.2.2. Interval model for the integrated system with wind farm

The simulation results for Case 3 and 4 by different optimization methods are listed in Table 5, and the power output intervals by units with different wind power uncertainty are shown in Figs. 16 and 17.

From Table 5, it can be found that for a certain wind power interval in Case 3, the objective cost by IO is between the corresponding values by SO and RO. The same situation is found in Case 4. Moreover, the expected costs for IO are close to the objective costs for SO while the objective costs for IO are a little less than the corresponding values for RO. In this regard, the proposed IO method can inherit the advantages of SO and RO and give consideration to both operation economy and reliability.

On the other hand, the increment of objective cost for IO in Case 4 is 16 573 $ and 21 285 $ with the wind power interval

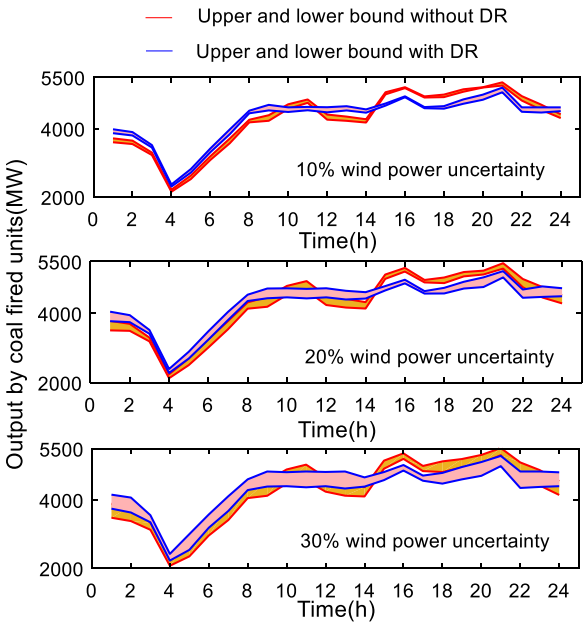

Fig. 17. The output interval of thermal units.

widening. By contrast, the corresponding increment for SO is 3541 $ and 3556 $, and the increment for RO is 17 465 $ and 25 475 $. It demonstrates that SO shows the worst sensitivity to wind power uncertainty while RO has the highest sensitivity to wind power fluctuation among the three optimization methods. And IO has moderate sensitivity to uncertainties, which can reduce the conservativeness caused by RO.

As shown in Figs. 16 and 17, the gap between the upper and lower bound by the gas-fired and thermal units becomes larger as the wind power uncertainty is increasing. And what is more, the scheduling power output in Case 3 shows higher volatility than that in Case 4, which results in greater unit operation cost.

6. Conclusions

An interval optimization based short-term dispatch model for the IES is established to coordinate the operation between natural gas system and power system. The proposed model integrates dynamic process of natural gas network, wind power uncertainty, demand response management for gas and electric loads. To investigate the performance of the proposed model, simulations for different cases are implemented in the 6-bus power system with 6-node natural gas system and the modified IEEE 118-bus system with 10-node natural gas system. The effect of demand response management, dynamic process of natural gas network, wind power uncertainty and installed capacity of wind farm are analyzed. The following conclusions can be obtained:

(1) Demand response management is an effective strategy to reduce the operation cost by changing the peak–valley characteristics of load curves.

(2) Considering the dynamic process of natural gas network can enhance the operation flexibility of the IES and wind power utilization.

(3) The interval optimization method only needs the upper/lower bound of wind power prediction to solve the coordination scheduling problem. Thus, it is a practicable and appropriate method to deal with uncertain variables with no need of the probability distribution hypothesis. Moreover, case studies demonstrate that the proposed IO method can give consideration to both economy and reliability, which can achieve superior performance compared to SO and RO.

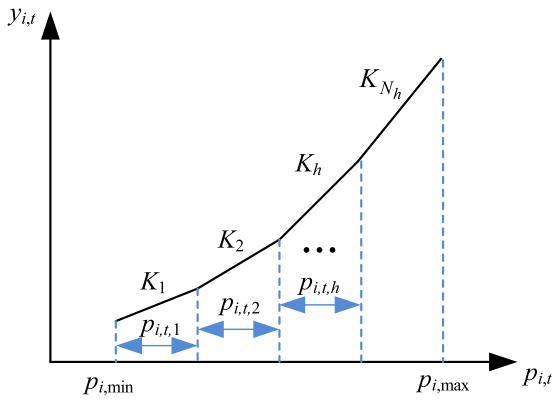

Fig. 18. Piecewise linearization of the quadratic terms.

Declaration of competing interest

The authors declare that they have no known competing financial interests or personal relationships that could have appeared to influence the work reported in this paper.

CRediT authorship contribution statement

Yachao Zhang: Conceptualization, Writing - review & editing. **Zhanghao Huang:** Data curation, Writing - original draft. **Feng Zheng:** Methodology, Supervision. **Rongyu Zhou:** Visualization, Investigation. **Xueli An:** Software. **Yinghai Li:** Validation.

Acknowledgment

This work was supported by National Natural Science Foundation of China (No. 61903088).

Appendix

The flow equation of natural gas pipeline expressed by Eq. (20) is nonlinear. In our study, the gas flow direction remains unchanged during the whole scheduling period, which is determined in advance. If $p_{i,t} \geq p_{j,t}$, Eq. (20) can be expressed as:

$$q_{ij,t}^2 = C_{ij}(p_{i,t}^2 - p_{j,t}^2) \tag{A.1}$$

The quadratic terms in Eq. (A.1) can be piecewisely linearized. Assuming that $y_{i,t} = p_{i,t}^2$, the linearization process can be described as follows:

$$\sum_{h=1}^{N_h} z_h = 1 \tag{A.2}$$

$$\sum_{h=l+1}^{N_h} z_h \leq N_h p_{i,t,l}/(p_{i,\max} - p_{i,\min}) \leq \sum_{h=l}^{N_h} z_h, \forall l \in \{1, 2, \ldots, N_h - 1\} \tag{A.3}$$

$$0 \leq N_h p_{i,t,l}/(p_{i,\max} - p_{i,\min}) \leq z_l, \forall l = N_h \tag{A.4}$$

$$p_{i,t} = p_{i,\min} + \sum_{h=1}^{N_h} p_{i,t,h} \tag{A.5}$$

$$y_{i,t} = p_{i,\min}^2 + \sum_{h=1}^{N_h} K_h p_{i,t,h} \tag{A.6}$$

where z_h is the introduced binary variable, the auxiliary variable $p_{i,t,h}$ represents the segment value of the continuous variable $p_{i,t}$ as shown in Fig. 18, K_h is the slope of the hth segment line, N_h is the number of the linear segments.

References

Alabdulwahab, A., Abusorrah, A., Zhang, X., Shahidehpour, M., 2015. Coordination of interdependent natural gas and electricity infrastructures for firming the variability of wind energy in stochastic day-ahead scheduling. IEEE Trans. Sustain. Energy 6 (2), 606–615.

Alham, M.H., Elshahed, M., Ibrahim, D.K., Zahab, E.E.D.A.E., 2016. A dynamic economic emission dispatch considering wind power uncertainty incorporating energy storage system and demand side management. Renew. Energy 96, 800–811.

Bai, L., Li, F., Cui, H., Jiang, T., Sun, H., Zhu, J., 2016. Interval optimization based operating strategy for gas-electricity integrated energy systems considering demand response and wind uncertainty. Appl. Energy 167, 270–279.

Carrión, M., Arroyo, J.M., 2006. A computationally efficient mixed linear formulation for the thermal unit commitment problem. IEEE Trans. Power Syst. 21 (3), 1371–1378.

Chaudry, M., Jenkins, N., Strbac, G., 2008. Multi-time period combined gas and electricity networkoptimisation. Electr. Power Syst. Res. 78 (7), 1265–1279.

Correa-Posada, C.M., Sánchez-Martín, P., 2015. Integrated power and natural gas model for energy adequacy in short-term operation. IEEE Trans. Power Syst. 30 (6), 3347–3355.

Correaposada, C.M., Sánchez-Martín, P., 2014. Gas network optimization, a comparison of piecewise linear models.

Dehghan, S., Amjady, N., Kazemi, A., 2014. Two-stage robust generation expansion planning, a mixed integer programming model. IEEE Trans. Power Syst. 29 (2), 584–597.

Geißler, B., Martin, A., Morsi, A., Schewe, L., 2012. Using piecewise linear functions for solving MINLPs. In: Mixed Integer Nonlinear Programming, Vol. 154. Springer, New York, pp. 287–314.

He, Y., Li, H., 2018. Probability density forecasting of wind power using quantile regression neural network and kernel density estimation. Energy Convers. Manage. 164, 374–384.

He, C., Liu, T., Wu, L., Shahidehpour, M., 2017. Robust coordination of interdependent electricity and natural gas systems in day-ahead scheduling for facilitating volatile renewable generations via power-to-gas technology. J. Mod. Power Syst. Clean Energy 5 (3), 375–388.

Jiang, R., Wang, J., Guan, Y., 2012. Robust unit commitment with wind power and pumped storage hydro. IEEE Trans. Power Syst. 27 (2), 800–810.

Li, G., Zhang, R., Jiang, T., Chen, H., Bai, L., Li, X., 2017. Security-constrained bi-level economic dispatch model for integrated natural gas and electricity systems considering wind power and power-to-gas process. Appl. Energy 194, 696–704.

Li, Y., Zou, Y., Tan, Y., Cao, Y., Liu, X., Shahidehpour, M., Tian, S., Bu, F., 2018. Optimal stochastic operation of integrated low-carbon electric power, natural gas and heat delivery system. IEEE Trans. Sustain. Energy 9 (1), 273–283.

Liu, K., Gao, F., 2017. Scenario adjustable scheduling model with robust constraints for energy intensive corporate microgrid with wind power. Renew. Energy 113, 1–10.

Liu, Y., Jiang, C., Shen, J., Hu, J., 2017. Coordination of hydro units with wind power generation using interval optimization. IEEE Trans. Sustain. Energy 6 (2), 443–453.

Liu, C., Lee, C., Shahidehpour, M., 2014. Look ahead robust scheduling of wind-thermal system with considering natural gas congestion. IEEE Trans. Power Syst. 30 (1), 544–545.

Liu, C., Shahidehpour, M., Fu, Y., Li, Z., 2009a. Security-constrained unit commitment with natural gas transmission constraints. IEEE Trans. Power Syst. 24 (3), 1523–1536.

Liu, C., Shahidehpour, M., Li, Z., Fotuhi-Firuzabad, M., 2009b. Component and mode models for the short-term scheduling of combined-cycle units. IEEE Trans. Power Syst. 24 (2), 976–990.

Liu, C., Shahidehpour, M., Wang, J., 2010. Application of augmented lagrangian relaxation to coordinated scheduling of interdependent hydrothermal power and natural gas systems. IET Gener. Transm. Distrib. 4 (12), 1314–1325.

Liu, C., Shahidehpour, M., Wang, J., 2011. Coordinated scheduling of electricity and natural gas infrastructures with a transient model for natural gas flow. Chaos 21, 025102.

Moore, R.E., 1979. Method and Application of Interval Analysis. SIAM, Philadelphia, PA, USA.

Nasrolahpour, E., Ghasemi, H., 2015. A stochastic security constrained unit commitment model for reconFigurable networks with high wind power penetration. Electr. Power Syst. Res. 121, 341–350.

Pinedo, M., 2007. Scheduling, Theory, Algorithms and Systems. Tsinghua University Press, Beijing.

Qadrdan, M., Wu, J., Jenkins, N., Ekanayake, J., 2013. Operating strategies for a GB integrated gas and electricity network considering the uncertainty in wind power forecasts. IEEE Trans. Sustain. Energy 5 (1), 128–138.

Qiao, Z., Guo, Q., Sun, H., Pan, Z., Liu, Y., Xiong, W., 2017. An interval gas flow analysis in natural gas and electricity coupled networks considering the uncertainty of wind power. Appl. Energy 201, 343–353.

Qin, S., Liu, F., Wang, J., Song, Y., 2015. Interval forecasts of a novelty hybrid model for wind speeds. Energy Rep. 1, 8–16.

Sengupta, A., Pal, T.K., 2000. On comparing interval numbers. Eur. J. Oper. Res. 127 (1), 28–43.

Siahkali, H., Vakilian, M., 2010. Fuzzy generation scheduling for a generation company (GenCo) with large scale wind farms. Energy Convers. Manage. 51 (10), 1947–1957.

Tan, Z., Ju, L., Reed, B., Rao, R., Peng, D., Li, H., Pan, G., 2015. The optimization model for multi-type customers assisting wind power consumptive considering uncertainty and demand response based on robust stochastic theory. Energy Convers. Manage. 105, 1070–1081.

Wardono, B., Fathi, Y., 2004. A tabu search algorithm for the multi-stage parallel machine problem with limited buffer capacities. European J. Oper. Res. 155 (2), 380–401.

Xiao, L., Wang, J., Dong, Y., Wu, J., 2015. Combined forecasting models for wind energy forecasting, a case study in China. Renew. Sustain. Energy Rev. 44 (17), 271–288.

Zeng, B., Zhao, L., 2013. Solving two-stage robust optimization problems using a column-and-constraint generation method. Oper. Res. Lett. 41 (5), 457–461.

Zhang, Y., Le, J., Zheng, F., Zhang, Y., Liu, K., 2019. Two-stage distributionally robust coordinated scheduling for gas-electricity integrated energy system considering wind power uncertainty and reserve capacity configuration. Renew. Energy 135, 122–135.

Zhang, Y., Liu, K., Liao, X., Qin, L., An, X., 2017. Stochastic dynamic economic emission dispatch with unit commitment problem considering wind power integration. Int. Trans. Electr. Energy Syst. 28 (1), e2472.

Zhang, X., Shahidehpour, M., Alabdulwahab, A., Abusorrah, A., 2015. Hourly electricity demand response in the stochastic day-ahead scheduling of coordinated electricity and natural gas networks. IEEE Trans. Power Syst. 31 (1), 592–601.

Zhang, T., Zhang, D., 2007. Agent-based simulation of consumer purchase decision-making and the decoy effect. J. Bus. Res. 60 (8), 912–922.